American Mineralogist, Volume 110, pages 1689-1701, 2025

High-resolution analysis of clay minerals and amorphous materials in martian analog environments

Michael T. Thorpe[1,2,*,†,‡], Elizabeth B. Rampe[2], Juergen Thieme[3,4], Eric Dooryhee[3], Seungyeol Lee[2,5], and Roy Christoffersen[6]

[1]University of Maryland, NASA Goddard Space Flight Center, and CRESST II, Greenbelt, Maryland 20771, U.S.A.
[2]NASA Johnson Space Center, Houston, Texas 77058, U.S.A.
[3]Brookhaven National Lab, NSLS-II, Upton, New York 11973, U.S.A.
[4]Institute for X-Ray Physics, Georg-August University Goettingen, Goettingen University, Göttingen 37073, Germany
[5]Department of Earth and Environmental Sciences, Chungbuk National University, Seowon-Gu, Cheongju, Chungbuk 28644, Korea
[6]Amentum JETS-II contract, NASA Johnson Space Center, Houston, Texas 77058, U.S.A.

Abstract

Mudrocks and mud-sized sediments (i.e., silt to clay) dominate the surface of Earth and Mars. These fine-grained sediments preserve a rich history of sedimentary processes from source to sink and shed light on ancient climates. However, both the physical and chemical nature of these materials make them difficult to fully characterize with traditional laboratory techniques. Here, we explore a cross-disciplinary and high-resolution approach using synchrotron radiation for X-ray diffraction, pair distribution function analysis, and submicrometer-scale X-ray fluorescence, combined with transmission electron microscopy, to better understand the nanostructure and composition of mud-sized sediments from a glacio-fluvial watershed in southwest Iceland. Our results demonstrate that sediments in the cold and wet climate of Iceland are more altered than previously thought, as evidenced by the identification of kaolinite and mixed-layer kaolinite-smectite. Additionally, sediments are enriched in amorphous materials and nanocrystalline phases, as determined from grain morphologies and compositions consistent with allophane, hisingerite, ferrihydrite, and halloysite. These alteration products are present as intimate mixtures that vary across depositional sites, demonstrating the dynamic nature of the secondary assemblage from source to sink. This work has implications for Mars, where, for example, basalt-sourced sedimentary rocks from Gale crater are abundant in clay minerals and amorphous materials. Finally, this work underpins the importance of using high-resolution techniques, a coordinated methodology, and developing innovative approaches for future planetary sample return missions (e.g., Mars sample return).

Keywords: Clays and amorphous materials, combine high-resolution analysis, sedimentary processes from source to sink, preparation for Mars sample return, Earth Analogs for Martian Geological Materials and Processes

Introduction

Mud and mudrock are blanket terms that refer to all siliciclastic sediments or sedimentary rocks with grain sizes predominantly of silt- (<63 μm) to clay-sized (<4 μm) particles (Hawkins and Pinches 1992; Prothero and Schwab 2004). On Earth, mudrocks represent the overwhelming majority of the sedimentary mass (Pettijohn 1975). Interestingly, Mars also has a rich repository of mudrocks, as illustrated by the stratigraphy of Gale crater. The Mars Science Laboratory (MSL) Curiosity rover has traversed over extensive (>800 vertical m) exposures of sedimentary rocks, including many outcrops inferred to be mudstones (e.g., Grotzinger et al. 2014, 2015). At the global scale, orbital imagery from the surface of Mars documents the remnants of depositional environments commonly associated with clay-sized detritus (e.g., deltaic and lacustrine) (Cabrol and Grin 2010). Furthermore, remote sensing data have identified the widespread occurrence of minerals inherent to the clay-size fraction (i.e., clay minerals) throughout the ancient terrains of Mars (e.g., Ehlmann and Edwards 2014). All these observations combined help further drive the significance of mudrocks in the martian sedimentary rock record. Additionally, Mars is covered in dust, with grain sizes ranging between 1 and 4 μm (Lemmon et al. 2019). Thus, the motivation to understand the composition of mud-sized sediment extends to surface fines and atmospheric dust on Mars.

Detailed characterization of the clay-size fraction may reveal the most information about both ancient environmental conditions and sedimentary processes, compared to its coarse-grained counterparts. For example, Nesbitt et al. (1996) demonstrated that terrestrial muds contain fewer primary minerals and are more chemically differentiated than coarser detritus. Similarly, Thorpe et al. (2021) compiled the mineralogy and geochemistry of the clay-size fraction from terrestrial fluvial sediments and weathering profiles around the globe to demonstrate a correlation between mean annual temperature and the extent of chemical weathering.

* Corresponding author E-mail: michael.t.thorpe@nasa.gov Orcid https://orcid.org/0000-0002-1235-9016

‡ Special collection papers can be found online at our website in the Special Collection section.

0003-004X/25/0011–1689$05.00/DOI: https://doi.org/10.2138/am-2023-9290

Another study from Rampe et al. (2022) explored the <2 μm fraction of proglacial sediments from the Collier Glacier in Oregon, U.S.A., and demonstrated that mineral composition was dominated by X-ray amorphous material(s), consistent with both primary glass and secondary alteration products. Together, these examples illustrate the unique information preserved in the mud fraction of sedimentary deposits.

While mud-sized sediment may be important for unraveling the sedimentary history of a planet and placing constraints on paleoclimates, these fine particulates are also the most difficult to analyze with traditional laboratory techniques. These difficulties stem from the small grain size and a complex mixture of clay minerals, poorly ordered phases, X-ray amorphous materials, nano-crystalline particles, and minute primary minerals. Some of these materials are sensitive to environmental changes as well as analytical exposure (e.g., Tosca et al. 2022). Thus, analyses of clay-sized sediments require careful sample preparation, high-resolution instrumentation, and sometimes increased analytical time to enhance the signal-to-noise ratio, but at other times, limited analytical dwell times are necessary because these materials are sensitive to the incident beam intensity.

In this study, we explore the clay-size fraction of glaciofluvial sediments from southwest Iceland with high-resolution analytical techniques. These same samples have been previously characterized with traditional laboratory analytical techniques (Thorpe et al. 2019). Previous results identified the prevalence of smectite and X-ray amorphous materials, with abundances on par with those observed by the CheMin XRD instrument on MSL (Thorpe et al. 2021). Expanding on these previous studies, the current investigation has two goals: (1) evaluation of a suite of high-resolution analytical techniques for characterizing the complex clay-size fraction and amorphous materials, and (2) development of a more comprehensive model for the origin and alteration history of fluvial sediments in Mars-analog mafic terrain under a cold climate.

Background

Iceland background and previous work

Iceland has been studied as a martian analog because basalt is the chief rock type in the region (e.g., Mangold et al. 2011; Ehlmann et al. 2012), and the contemporary climate of Iceland may be analogous to the martian paleoclimate (e.g., Gale crater; Thorpe et al. 2021). Exploring sedimentary processes in these basaltic terrains has shed light on how mafic detritus is transformed from source to sink (e.g., Thorpe et. al. 2019); however, the clay size fraction of these sediments remains only partly characterized.

The sediments from this study originated in the central highlands of Iceland with the Lake Hvítárvatn, a proglacial lake fed from two outlet channels of meltwater from the Langjökull glacier (Fig. 1). This lake feeds the Hvítá river, and further downstream, other tributaries funnel into this fluvial system, turning it into the Hvítá S branch. In total, sediments in this system can travel ~130 km from source to sink and descend 428 m before discharging into the North Atlantic Ocean. Sediments previously analyzed by Thorpe et al. (2019) will be the focus of this work, which builds upon previous bulk analyses. The sediment samples consisted of fluvial deposits in the upper reaches of the watershed, detritus downriver along the transportation pathway, and sediments approaching the delta, referred to throughout the text as source terrains, downstream, and delta, respectively. These sites were selected largely to track compositional transformations in the sediment as it progressed downstream. Online Materials[1] Table S1 includes the coordinates and the previous analysis conducted on these sediments. Additionally, an Icelandic basalt, sampled in the mountainous terrains near the glacier, was also characterized and classified as the "source rock." However, we recognize that the source is likely more diverse than this individual sample, and this particular source rock is meant to serve as a comparison of an igneous lithology with primary minerals and basaltic glass to secondary alteration products in the sediment deposits.

The geochemistry and mineralogy of various grain size fractions and the source rocks from the Hvítá watershed document a complex history involving chemical weathering, sediment sorting, and provenance mixing (Thorpe et al. 2019). The mass fraction of the clay-size fraction and alteration phase abundances increase downstream, suggesting continued alteration within the fluvial system. The geochemical measurements on these sediments demonstrated a fractionation of elements from source to sink, e.g., sediments approaching the river delta were most enriched in iron. Here, we address outstanding questions from the earlier study: (1) what discrete phases make up the abundant amorphous fraction of these mafic-derived sediments; (2) can the elemental cycling in the sedimentary system be linked to alteration along the sediment transportation pathway; and (3) what can we learn about the sedimentary processes from source to sink in the cold climate of Iceland through detailed analysis of the clay size fraction?

Amorphous vs. crystalline terminology

We follow the definitions of crystalline and amorphous materials in Caraballo et al. (2015) and Smith and Horgan (2021). Broadly, crystalline phases have atomic arrangements that repeat periodically in three dimensions (i.e., unit cell), and this atomic order extends over tens of nanometers (Caraballo et al. 2015; Smith and Horgan 2021). Amorphous materials lack long-range atomic order but can often have predictable distances between atoms and the nearest neighboring atom, thus exhibiting a short-range order at scales < ~10 nm (Caraballo et al. 2015; Smith and Horgan 2021). With these end-member definitions in mind, there is also a transition between crystalline and amorphous that includes nanocrystalline materials, which can also be described as nanoscale and poorly crystalline, paracrystalline, or polyphasic. These nanocrystalline materials contain crystalline domains on the scale of nanometers (Caraballo et al. 2015; Smith et al. 2021). Discretely identifying nanocrystalline and amorphous materials can be challenging with traditional laboratory techniques and underpins the importance of investigating these materials with high-resolution analytical approaches.

Characterizing clay minerals, amorphous phases, and nanocrystalline materials

Determining the physiochemical properties of clay minerals and amorphous and nanocrystalline materials is a critical challenge for scientists today; however, different characterization techniques can provide a partial picture of the true nature of these

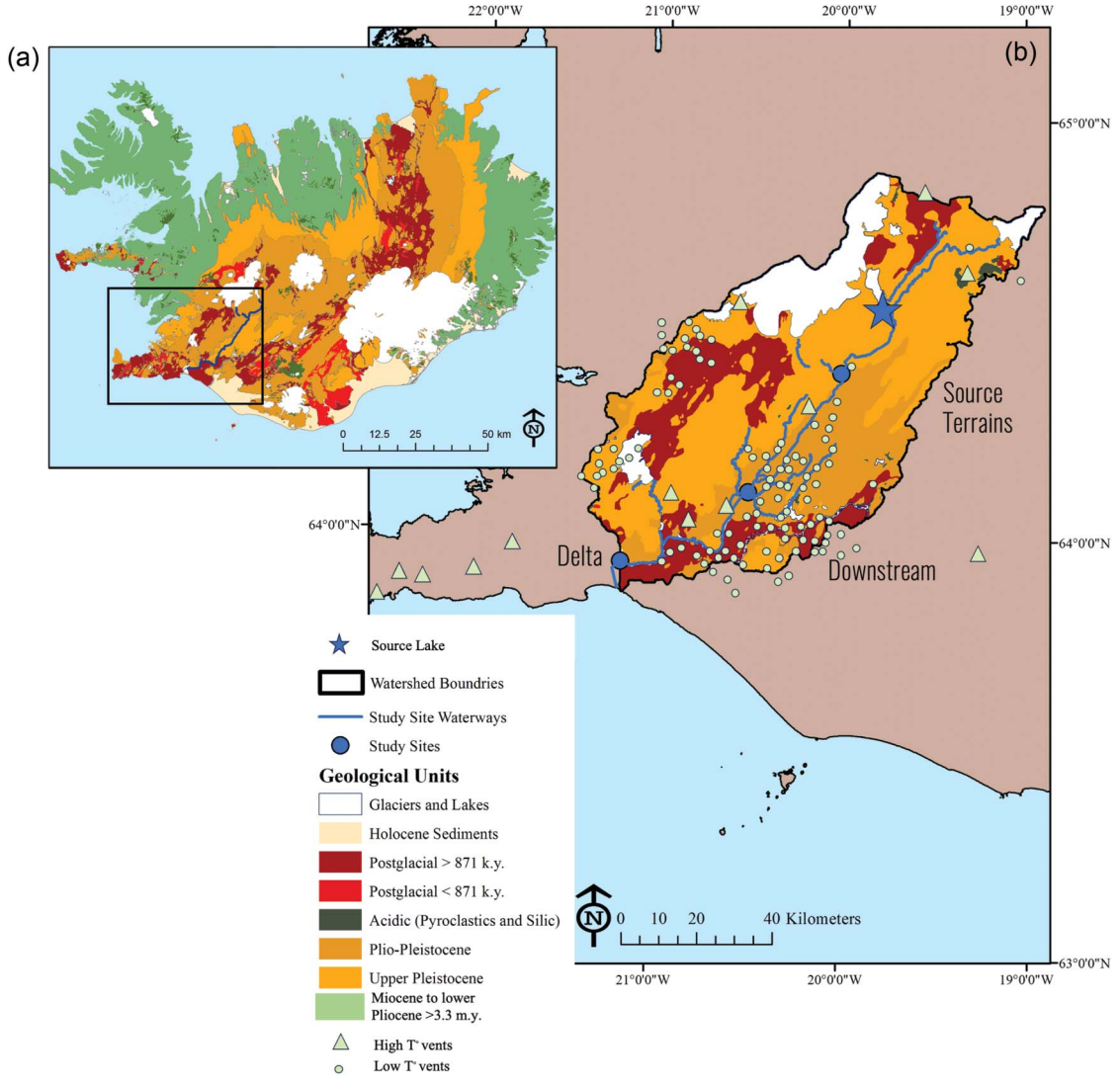

Figure 1. Geological map of Iceland modified from Thorpe et al. (2019) (**a**) with an insert displaying the Hvíta watershed and samples interrogated in this study (**b**). Also highlighted on the insert map are high- and low-temperature (*T*) hydrothermal vents to investigate alteration product input to the system. The location of these vents was obtained from Bodvarsson (1961).

alteration products (Modena et al. 2019). For example, transmission electron microscopy (TEM) is a powerful technique that has been employed in clay mineralogy for decades and enables the microstructural and morphologic characterization of clay minerals and amorphous materials (e.g., Brown and Rich 1968; Dixon and McKee 1974; Malla and Komameni 1990; Liu et al. 2019; Modena et al. 2019). X-ray diffraction (XRD) is a powerful and nondestructive tool that characterizes crystal structure and provides abundances of amorphous materials (e.g., Petkov 2008; Bunaciu et al. 2015; Modena et al. 2019). Pair distribution function (PDF) analysis is a specialized approach that enables the determination of structural information, including nearest neighbor atomic distances and coordination numbers, for clay minerals and poorly to non-crystalline materials (e.g., Klug and Alexander 1974; Petkov 2008). Another approach, submicrometer-scale X-ray fluorescence (SRX), is used to characterize the elemental composition of nanoparticles. This method has the unique ability to capture microheterogeneities of nanoparticle chemical compositions (e.g., De Andrade et al. 2011; Chen-Wigegart et al. 2016; Allwood et al. 2018).

Methods

The approach used in this research combines TEM, synchrotron powder XRD, synchrotron X-ray PDF, and synchrotron SRX to characterize the nanoscale structure, morphology, and elemental composition of the clay size fraction, similar to the approach employed in Modena et al. (2019). The sediments subjected to all these techniques were first separated from the bulk sediment by dry sieving to <45 μm. The <1 μm was then separated using a settling column and Stoke's Law.

TEM imaging

For TEM, sediments were embedded in epoxy and sectioned using ultramicrotomy to produce thin sections ~50 nm thick. TEM was carried out using a JEOL JEM-2500SE field-emission scanning transmission electron microscope (FE-STEM) at NASA Johnson Space Center. Bright-field TEM images, high-resolution TEM (HRTEM) images, and fast Fourier transform (FFT) were acquired from

ultra-microtomed sections. Chemical compositions were characterized using a JEOL SD60GV 60 mm^2 ultra-thin window silicon drift detector (SDD).

Synchrotron XRD and PDF analyses

For synchrotron XRD and PDF, powders were loaded into Kapton capillaries (1 mm ID Polyimide Tubing), trimmed to ~50 mm in length, and sealed with a standard clay plug. Samples were analyzed on the 28-ID-1 beamline at the National Synchrotron Light Source II (NSLS II), Brookhaven National Laboratory (BNL). The incident X-ray beam energy was ~63.6 keV, with a corresponding X-ray wavelength of 0.19316 Å. In addition to analyzing the samples, clay mineral standards from the Clay Mineral Society were analyzed under the same conditions to aid in clay mineral classifications. The <2 μm separate of a montmorillonite (SAz-1), nontronite (NAu-1), and saponite (SapCa-1) were characterized via XRD and PDF. Finally, empty capillaries with the standard clay plug were analyzed to account for any peaks not associated with phases within our sample.

Rietveld analyses of the XRD patterns using the MDI Jade software produced relatively good fits (Online Materials[1] Fig. S1), but these results are semi-quantitative. Quantifying clay mineral abundance using XRD patterns of standards as an overlay in the refinement requires the calculation of reference intensity ratios, which was not performed as part of this work. Furthermore, we did not add a standard in known quantity (e.g., corundum) to our samples, making it impossible to quantify the abundance of non-crystalline materials. To further interpret the XRD patterns, we also modeled the clay mineral phases present using the NEWMOD software, a program developed for calculating one-dimensional diffraction patterns for mixed-layer clay minerals (Moore and Reynolds 1989). PDF patterns were processed at NSLS II, where two-dimensional patterns were converted to one-dimensional patterns using FIT2D to determine geometric parameters and radial integrations (Hammersley et al. 1994). The techniques for analyzing well-crystalline phases have been well established using the reduced atomic PDF, G(r), which normalizes the PDF by a spherical area (Petkov 2012; Terban and Billinge 2021). These G(r) calculations were completed at NSLS II using the PDFGETX2 program (Qiu et al. 2004), where standard corrections and an area-to-detector geometry were applied (Chupas et al. 2003). We note that fitting standard phases using linear models of PDF patterns was difficult due to the natural complexity of these Icelandic samples. Thus, for this work, we also qualitatively compared standards run at the synchrotron at the same time as the sample analysis.

SRX and XANES characterization of elemental composition

For SRX, the loose sediments were mounted on high-purity silica glass slides with an ultrapure epoxy. Although these loose grains were <1 μm, the particles tend to flocculate, resulting in larger conglomerations of smaller grains. This sample preparation technique was beneficial for locating scanning areas for XRF and provided a way to reference our target areas. The SRX beamline at NSLS II is an undulator beamline located at sector 5-ID, offering an incident X-ray beam energy range of 4.5 to 20 keV. The 5-ID SRX beamline provides the unique capability of performing high-resolution XRF mapping as well as X-ray absorption near-edge structure (XANES) spectroscopy. Both these capabilities were employed in this study. Due to the small spot size of the SRX beam, we were unable to scan the entire thin section; instead, we focused on arbitrarily selected locations with a significant particle density, ultimately providing useful randomness in sampling to investigate heterogeneity. After selecting a dense area of particles on the thin section, an SRX map scan was performed on a selected target area. These SRX maps were then analyzed in real-time for elemental relationships, and either an additional, tangential map was created, which would later be stitched together, or select regions of interest (ROI) were further interrogated with SRX beamline capabilities. For these ROIs, we zoomed in and performed quick "XANES-like" mapping that targeted the energy windows of the various Fe-oxidation states (i.e., Fe^{3+} and Fe^{2+} at 7.133 and 7.1215 eV, respectively). By targeting these energy windows, anything above the adsorption edge was excluded; thus, we could focus on a discrete oxidation state and perform a rapid analysis. This was a new approach for sedimentary deposits, referred to throughout the text as SRX XANES maps, which reduced the beam damage from extended dwell times on sensitive phases (e.g., clay minerals, nanocrystalline phases, and amorphous materials). SRX XANES maps were compared to traditional XANES scans. To compare these approaches, first, a rapid SRX XANES map was completed, and then traditional XANES scans were acquired at points within a grain that were identified from the SRX XANES maps as having variable oxidation states.

Results

Microstructural characterization by TEM

Crystalline phases. Nanoprobe investigation using TEM identified discrete microstructures, variations in textures and morphology, and an overall contrast between particles in each of the sediment deposits. Moreover, each deposit along the transportation pathway displayed a unique composition in the bright-field diffraction contrast and high-resolution lattice fringe imaging (Fig. 2). From TEM images, we identified a 12.5 Å phase in all sediment deposits and both a 12.5 and 15 Å phase in the downstream and delta sediments, consistent with smectite clay minerals with different levels of interlayer hydration. Moreover, from a fast Fourier transform (FFT) of the downstream sediments, we identified the interstratification of a 7.1 and 12.5 Å phase (Fig. 3), suggesting the presence of mixed-layer kaolinite/smectite (K/S).

Amorphous and nanocrystalline materials. We identified four main categories or phases of amorphous materials and nanocrystalline phases through qualitative assessment of TEM images of some regions that lack lattice fringes. We then grouped these regions based on morphology and their relative abundance based on their volumetric distribution in the TEM images. Particles with a needle-like or tubular structure likely represent a halloysite-like phase, a 1:1 layer structure clay mineral (e.g., Kogure 2016). This halloysite-like phase was identified in both the source terrains and delta sediments. We also observed groups of particles that have a cloud-like structure similar to allophane (Filimonova et al. 2016; Du et al. 2022), which were identified in the source terrains and downstream sediments. Some particles in the Icelandic sediments have a curved or circular morphology, similar to hisingerite (Eggleton and Tilley 1998), and these particles were only identified in the source terrains. Finally, we identified cloud-like particles intimately mixed with a darker particle, likely representing ferrihydrite. This morphology of ferrihydrite has been observed in other studies with high-resolution TEM images, where agglomeration of ferrihydrite nano-domains was observed as an incipient weathering product of basaltic glass (e.g., Schindler et al. 2019). Ferrihydrite is observed in all sediment deposits; however, the ferrihydrite clouds become more rounded going downstream.

XRD results

Crystalline phases and amorphous abundances.. Synchrotron XRD patterns displayed sharp peaks consistent with well-crystalline primary phases from a basaltic source, i.e., plagioclase, olivine, and pyroxene (Fig. 4). The peaks associated with these primary phases are less abundant in the downstream and delta sediments, consistent with previous work on the bulk sediments (Thorpe et al. 2019) (Online Materials[1] Fig. S2). We identified two clay minerals with peaks at 7.1 and ~12.4 Å in synchrotron XRD patterns, neither of which was previously identified in the Icelandic clay sediments using laboratory XRD [i.e., Thorpe et al. (2019), random powder mounts]. The position of these peaks is consistent with the presence of smectite and kaolinite, confirming the identification from TEM. Additionally, we observe a subtle peak at ~19.5 Å, which could be from regularly stratified mixed-layer K/S. However, this peak

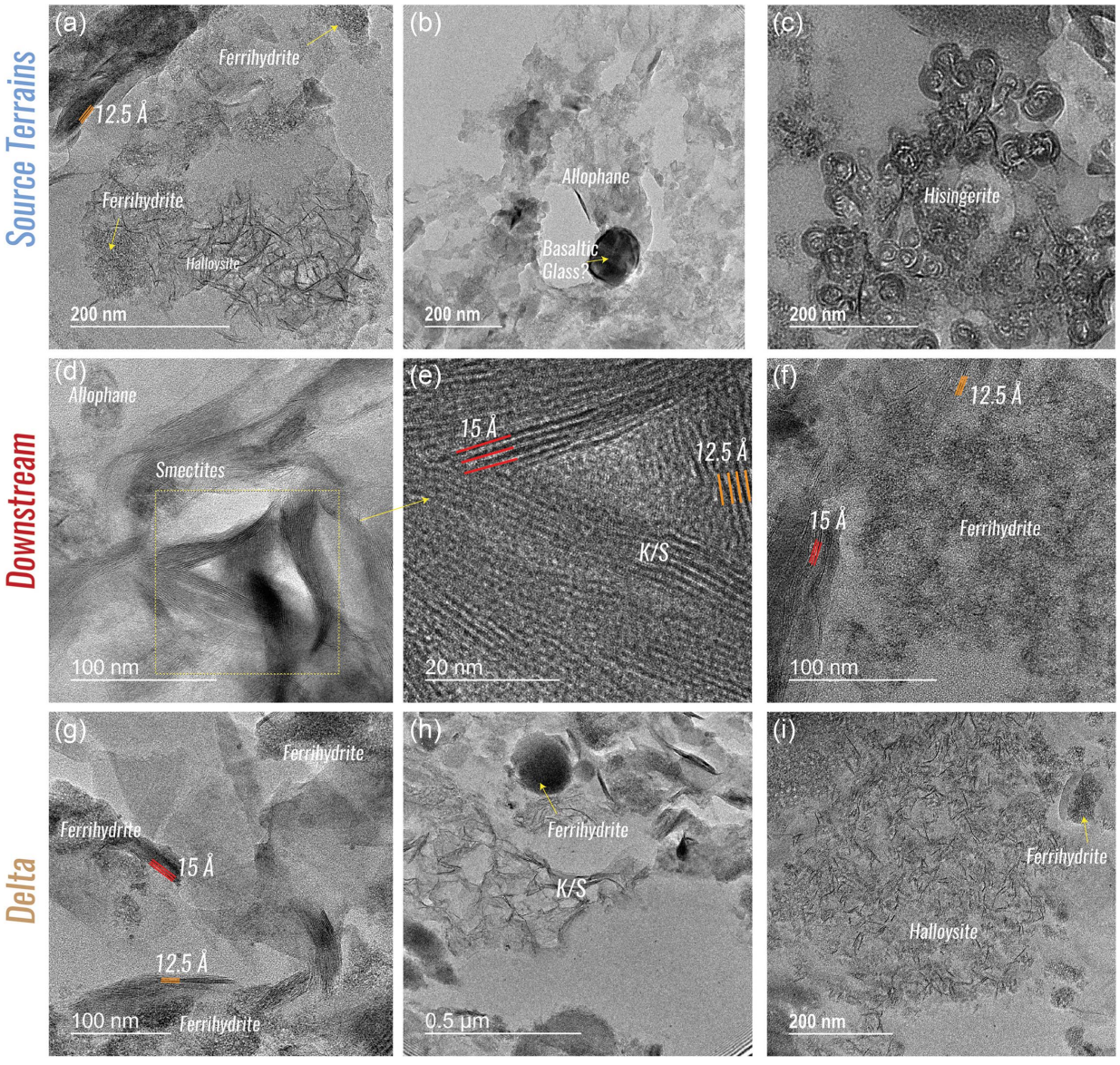

Figure 2. Bright-field diffraction contrast and high-resolution lattice fringe imaging from our TEM analysis. K/S represents the mixed-layer kaolinite-smectite phase.

is close to the beamstop, and depending on how the beamstop shadow is masked, this peak may be an instrument artifact. Thus, future investigations should target an approach that can use synchrotron XRD to aid in unraveling mixed-layer clay minerals with a superstructure peak. Examples of such approaches may include slightly lower energy ranges to constrain the beamstop shadow and/or a variable distance between the beamstop and detector.

To help identify the discrete smectite phase observed in the XRD patterns, we compared 001 and 060 peak positions of standard clay minerals to our samples (Fig. 4; Online Materials[1] Fig. S3). Based on TEM imaging of smectite present with variable hydration states, we used the NEWMOD software to create a clay mineral mixture to best model the 001 reflection. In this model, we were able to recreate the smectite 001 reflection and determine a relative ratio of 12:1 for smectites with two water layers to smectites with one water layer (Online Materials[1] Fig. S4). Analyses of the 060 reflection (Fig. 4c), which provides details on the octahedral coordination, show this peak is typically broad in the Icelandic sediments, suggesting a mixture of clay minerals. The 7.1 Å peak is consistent with kaolinite or a serpentine phase, however, both the 001 and 060 reflections for the Icelandic sediments are a better match with kaolinite (Fig. 4). Based on a qualitative assessment of peak intensity, which is directly correlated with phase abundance, the downstream and delta sediments contain the highest abundances of smectite and kaolinite. XRD results suggest that X-ray amorphous abundances also increase as a function of distance from the source based on the relative scatter above the baseline, centered around 5 Å.

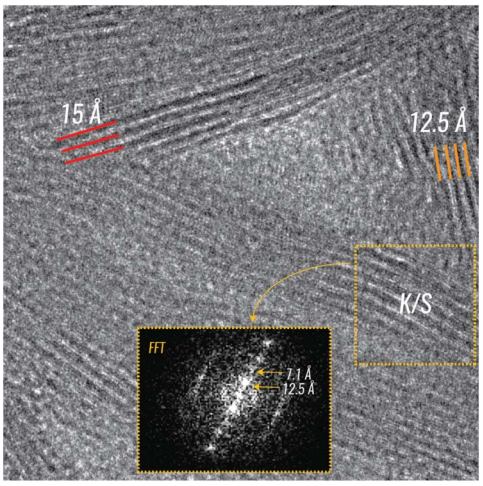

Figure 3. Bright-field diffraction contrast and high-resolution lattice fringe imaging from our TEM analysis, focusing on a location in the downstream sediments in which two different smectites are intimately mixed with the mixed layer clay mineral, kaolinite-smectite (K/S).

PDF clay and amorphous characterization

Strong PDF peaks in our source rock sample indicate that it contains more crystalline phases than the sediment deposits (Fig. 5). This supports the XRD analyses from both the previous study (Thorpe et al. 2019) using the bulk sample and this work focusing on the <1 μm fraction, both suggesting that X-ray amorphous materials become more abundant as a function of distance from the source (Fig. 4).

PDF patterns are consistent with multiple phases within each sediment sample, consistent with the identification of multiple non-crystalline materials in TEM (Fig. 2). For this work, we compared the sediment and source rock PDF patterns to that of a set of standards run under the same conditions, thus allowing us to identify major phases contributing to the PDF pattern (Fig. 5). Characterizing the chemical variations in these complex samples will require additional modeling beyond the scope of this paper and could be resolved with future least-squares optimization to deconvolve the individual components for amorphous and nanocrystalline material mixtures (Jibrin et al. 2024).

The PDF pattern of the source rock is consistent with opal or silica glass, possibly representing a primary volcanic glass. An opal peak is observed in the source terrain sediment but not observed in the downstream or delta PDF patterns. We observe peaks that are correlated with ferrihydrite and nontronite in the downstream and delta sediments. Nontronite is consistent with the strong ~12.5 Å XRD peak in the downstream XRD pattern (Fig. 4). XRD and PDF data demonstrate that nontronite has a more intense peak in the downstream sediment compared to the delta deposit. Like nontronite, PDF patterns suggest that ferrihydrite increases in abundance with distance traveled. PDF patterns are consistent with kaolinite in the fluvial sediments as either a discrete peak or a shoulder to a nearby peak.

SRX elemental composition

High-resolution elemental maps using SRX demonstrate Fe and Ca are abundant in all sediments (Fig. 6). This is not surprising, as Fe and Ca may be hosted in many primary mafic minerals (e.g., olivine, plagioclase, and pyroxene). However, the distribution of Fe and Ca may provide clues to the sedimentary story. For example, Fe and Ca are often co-located, but in the source terrains and downstream sediments, Fe is abundant throughout the sample, whereas Ca is restricted to grains with distinct boundaries. We hypothesize that these discrete grains are well-crystalline detrital phases (e.g., plagioclase). Further support for detrital mafic minerals in the <1 μm sediments can also be seen in selected hot spots of Ni, Cu, and Co, which are elements that are easily substituted into olivine and a phase that is most abundant in the headwaters. In contrast, in downstream sediments, the co-location of Fe and Ca is more dispersed, which may represent the incorporation of both Fe and Ca into alteration products, such as smectites. Downstream, we also see a strong correlation between Fe and Mn, which may both exist in olivine or alteration products (e.g., clay minerals). If that latter scenario were true, then this observation could potentially record redox-sensitive processes within the source-to-sink system. Finally, the delta sediments display an overall rounding of particles and a relative homogenization of elemental distribution. A change in particle roundedness with distance from the source was also observed in TEM images (Fig. 2), where the microstructure of the ferrihydrite grains changes as a function of distance from the source.

In addition to these high-resolution maps, we also experimented with creating Fe-oxidation state maps using the rapid SRX XANES maps approach. The results of the Fe-oxidation maps outline particles in the downstream and delta sediments that display an exterior enriched in Fe^{3+} and an interior concentrated in Fe^{2+} (Fig. 7). This observation of Fe-oxidation states may suggest that a weathering rind is forming on these particle grains within the sedimentary system. To test this SRX XANES map approach vs. the traditional XANES technique, we explored additional grains that displayed similar features of zonation. Results from the traditional XANES scans displayed no change in oxidation state. In fact, after the traditional XANES scans were completed, a subsequent rapid SRX XANES map was reacquired, and the grain was homogenized, with no oxidation state zonation, suggesting that beam damage had occurred to the analytically sensitive phases within these sediments.

Discussion

A combined high-resolution analysis of the clay size fraction of Icelandic sediments complements our previous study (Thorpe et al. 2019) by providing more information on the sedimentary history. For example, TEM enabled the identification of three new clay mineral phases and an assortment of both amorphous materials. Similarly, the identification of new peaks in the synchrotron XRD patterns indicates a deficiency in bulk laboratory analyses and provides a new clue for interpreting geological history, as discussed below. As we extend our knowledge base to Mars, we can better constrain the potential clay and amorphous compositions and prepare to analyze samples collected by return missions with similar high-resolution approaches.

The clay mineral story

The clay mineral story in Iceland is complex and involves smectite from various soils throughout the island (Wada et al. 1992),

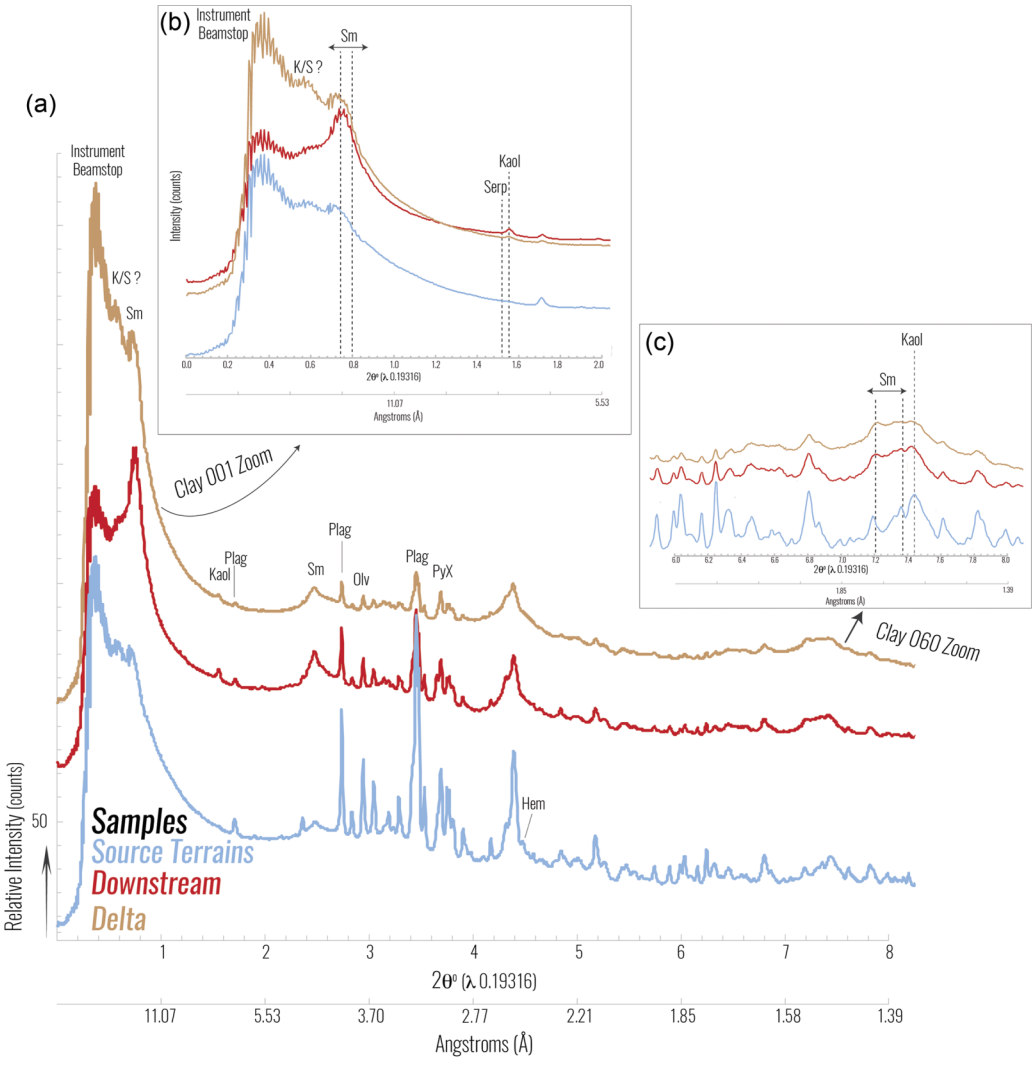

Figure 4. Synchrotron XRD patterns of samples (**a**). Panel (**b**) zooms into the important clay mineral 001 reflections as well as the new superstructure peak and (**c**) focuses on the 060 reflection important to distinguish the octahedral site occupancy for clay minerals. Mineral abbreviations are for plagioclase (Plag), olivine (Olv), pyroxene (PyX), hematite (Hem), smectite (Sm), kaolinite (Kaol), and serpentine (Serp). K/S, identified in the text as kaolinite-smectite, is labeled with a question mark because of its proximity to the beamstop, but the position of a peak here in the XRD data would also be consistent with mixed-layer clay mineral previously identified with TEM. Peak locations for clay mineral standards also run at the 28-1D beamline are displayed in black dashed lines as well as the peak locations of kaolinite and serpentine. Montmorillonite, kaolinite, and serpentine reference patterns are from the American Mineralogist Crystal Structure Database (Downs and Hall-Wallace 2003).

smectite in glacio-fluvial sediments (e.g., Thorpe et al. 2019), kaolinite in subglacial hydrothermal systems (Warner and Farmer 2010), and a kaolinite/smectite phase from hydrothermal sediments (Dekov et al. 2005; Markússon and Stefánsson 2011). To add to this story, we report multiple smectites (i.e., crystal structures with 12.5 and 15 Å interlayer spacings), kaolinite, and an interstratified clay phase in glacio-fluvial sediments. These findings may suggest that the surficial weathering history from source to sink is more dynamic than previously thought. For example, the difference in basal spacing for the smectites observed in TEM images and XRD patterns suggests different amounts of water in the interlayer site. This observation could be a product of sample preparation and relative humidity or a result of various cations in the interlayer site (e.g., Li^+, Na^+, K^+, Ca^{2+}, and Mg^{2+}). The relationship between the number of adsorbed water molecules is related to the nature of the interlayer cation (Suquet et al. 1975). Thus, in the Icelandic sediments, the 12.5 Å smectite would have an interlayer cation with lower hydration energy (e.g., Na^+), and the 15 Å smectite would have an interlayer cation with higher hydration energy (e.g., Mg^{2+}). The occurrence of two smectitic phases could suggest a transformation via cation exchange during transport (Meunier 2005).

In addition to the smectite diversity, the identification of kaolinite may suggest that the degree of weathering in the sediments is more advanced than previously documented. We propose this scenario because in nature, weathering reactions commonly alter smectite into kaolinite (Środoń 1999). However, we recognize that the Hvítá watershed is vast, ultimately sampling a

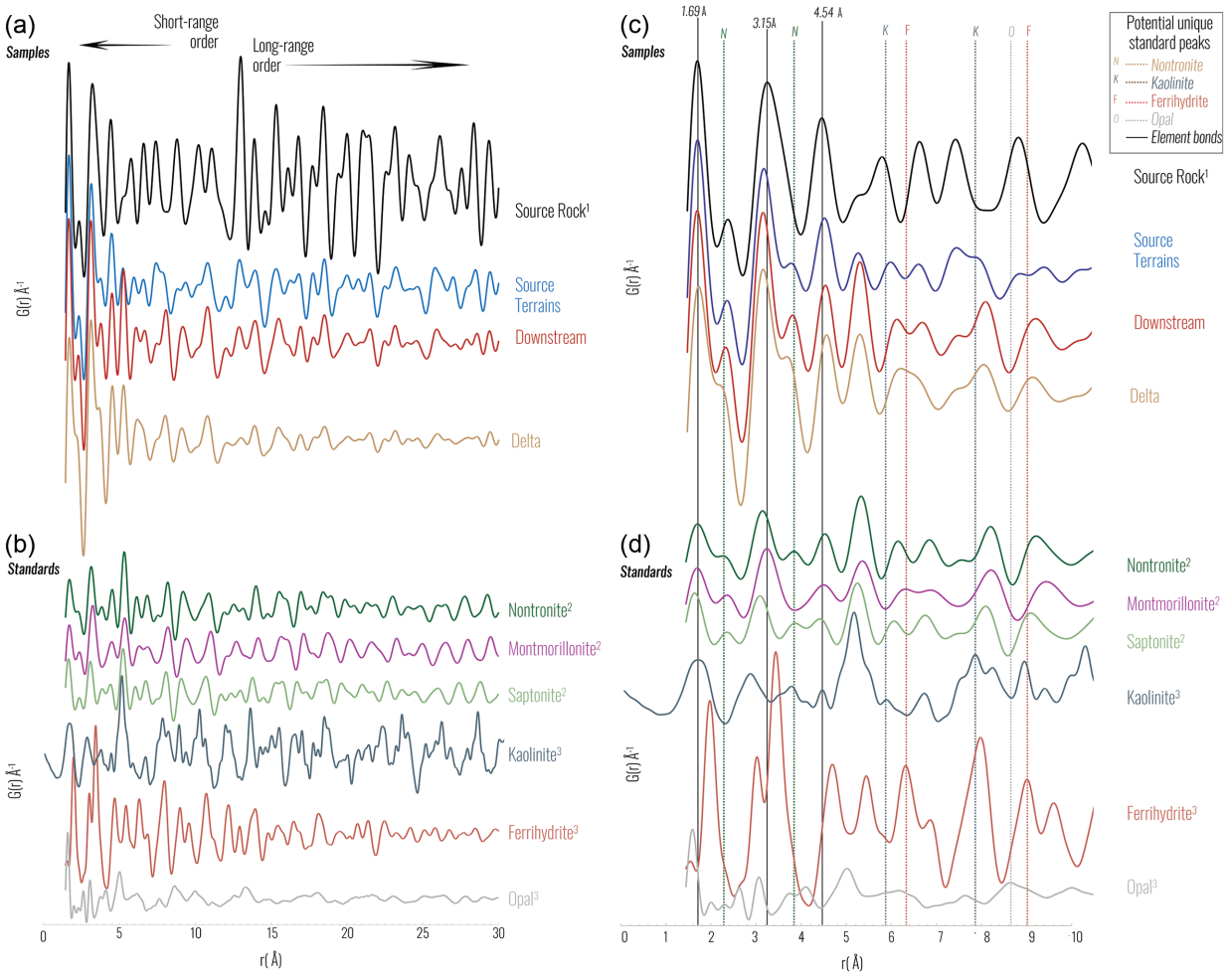

Figure 5. PDF patterns for the Icelandic sediments and a representative Icelandic basalt (Thorpe et al. 2019) serving as the "source rock" comparison. Also plotted are standards that were run at the same time of the analysis to serve as a reference from peaks within the PDF patterns. References: [1]Thorpe et al. 2019, [2]Clay Mineral Society standards; [3]Lee and Xu 2020; [4]Lee et al. 2022.

significant surface area from source to sink, including hydrothermal systems (Fig. 1). Thorpe et al. (2019) documented at least one additional evolved igneous source contributing to the system based on rare earth element (REE) patterns and trace element trends. Moreover, recent work in Iceland has demonstrated that detailed exploration of the provenance in smaller catchments that feed into the Hvítá watershed is even more complex than previously reported (Putnam et al. 2024). Thus, while this catchment is dominated by a progenitor with a basaltic composition, as inferred from historical geological maps (Fig. 1), the incorporation of other igneous parent rocks (e.g., andesites) or altered sources (e.g., hydrothermal inputs) cannot fully be ruled out and may be a source of kaolinite (Dekov et al. 2005; Markússon and Stefánsson 2011). We believe that kaolinite formed in situ in the Hvítá from subaerial weathering because there is limited evidence for other hydrothermal inputs. For example, at hydrothermal vents in Iceland, kaolinite occurs in the high activity zones, i.e., where pH is lowest and temperature is highest (Markússon and Stefánsson 2011; Sánchez-García et al. 2020). In these zones, kaolinite is commonly associated with pyrite and anatase, two phases absent from our previous study in the bulk sediments as well as the high-resolution results presented here. Additionally, the increase in kaolinite abundance with distance from the source suggests that a sedimentary process influences its abundance. Finally, the identification of K/S in TEM images of downstream sediments may be a transitional phase between smectite and kaolinite. Together, this clay mineral story may suggest that weathering is progressing throughout the transportation processes from source to sink, instead of solely in the source terrains or within the sedimentary basin. Thus, while we cannot rule out hydrothermal input(s) to the system, we favor chemical weathering as the process leading to both kaolinite and the K/S phase.

The amorphous conundrum

Amorphous materials have historically been a challenge to characterize, both on Earth (e.g., Ashley 1909; Colman 1982; Wada 1987; Dixon and Weed 1989; Arnalds 2004; Smith and Horgan 2021; Rampe et al. 2022) and on Mars (e.g., Dehouck et al. 2014; Achilles et al. 2020; Smith et al. 2021, 2022). This

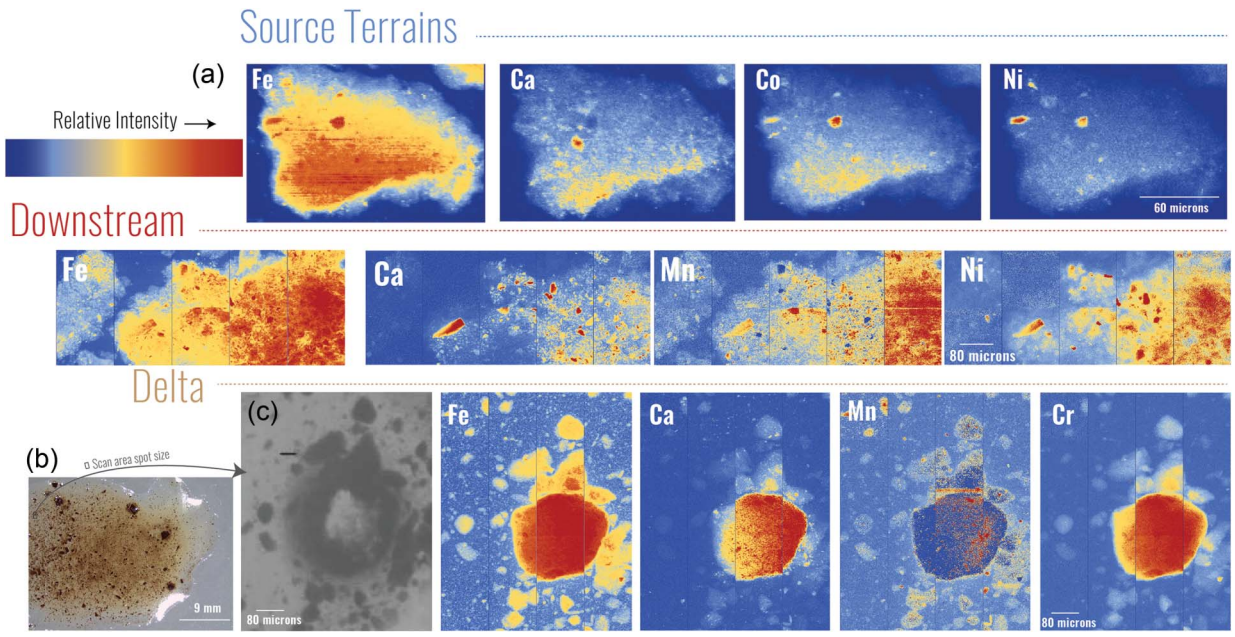

Figure 6. SRX elemental maps. A color ramp is used to display relative intensity within each sample site analysis, with red indicating more intense elemental concentrations and blue representing less abundant contents.

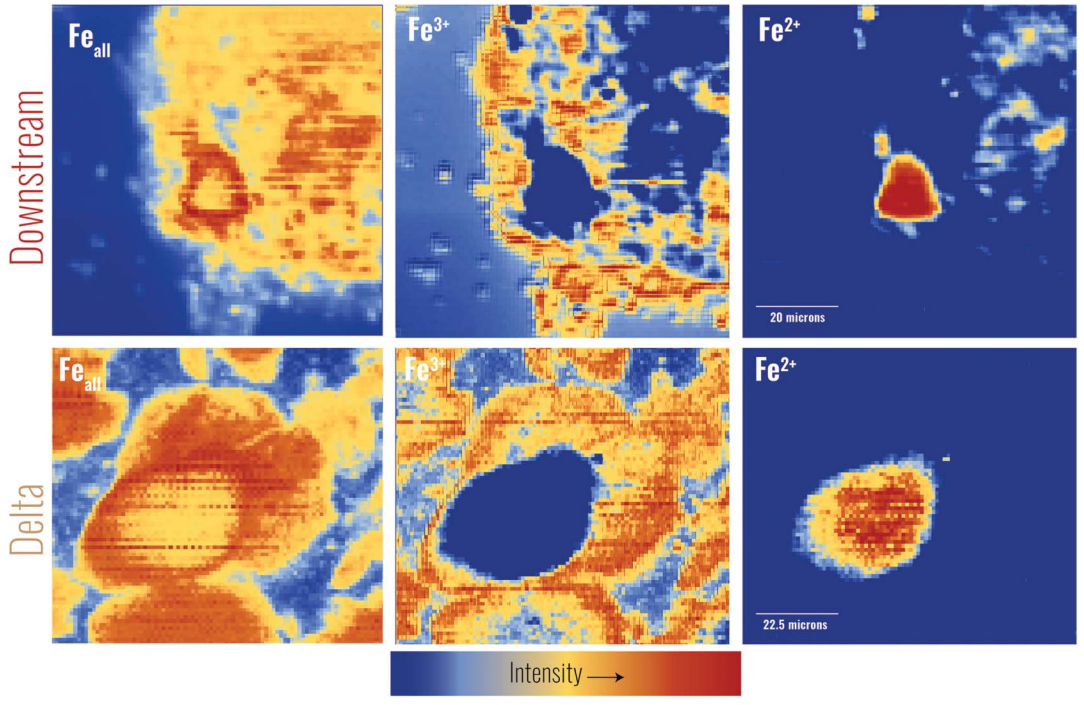

Figure 7. SRX Fe-oxidation maps. An intensity color ramp is used with red indicating more intense concentrations and blue representing less abundant contents.

hardship has even led authors like McLennan et al. (2019) to deem it as the "amorphous conundrum" for Mars. Part of the reason why amorphous materials are difficult to characterize on Mars is that they are likely a mixture of multiple amorphous materials and nanocrystalline phases, and the individual components are difficult or impossible to separate using orbital and in situ mineralogical measurements (e.g., XRD, infrared spectroscopy).

In this study, we observe that glacio-fluvial sediments from Iceland are an intimate mixture of at least four nanocrystalline phases and amorphous materials. These phases include allophane with a cloud-like morphology, ferrihydrite with Fe

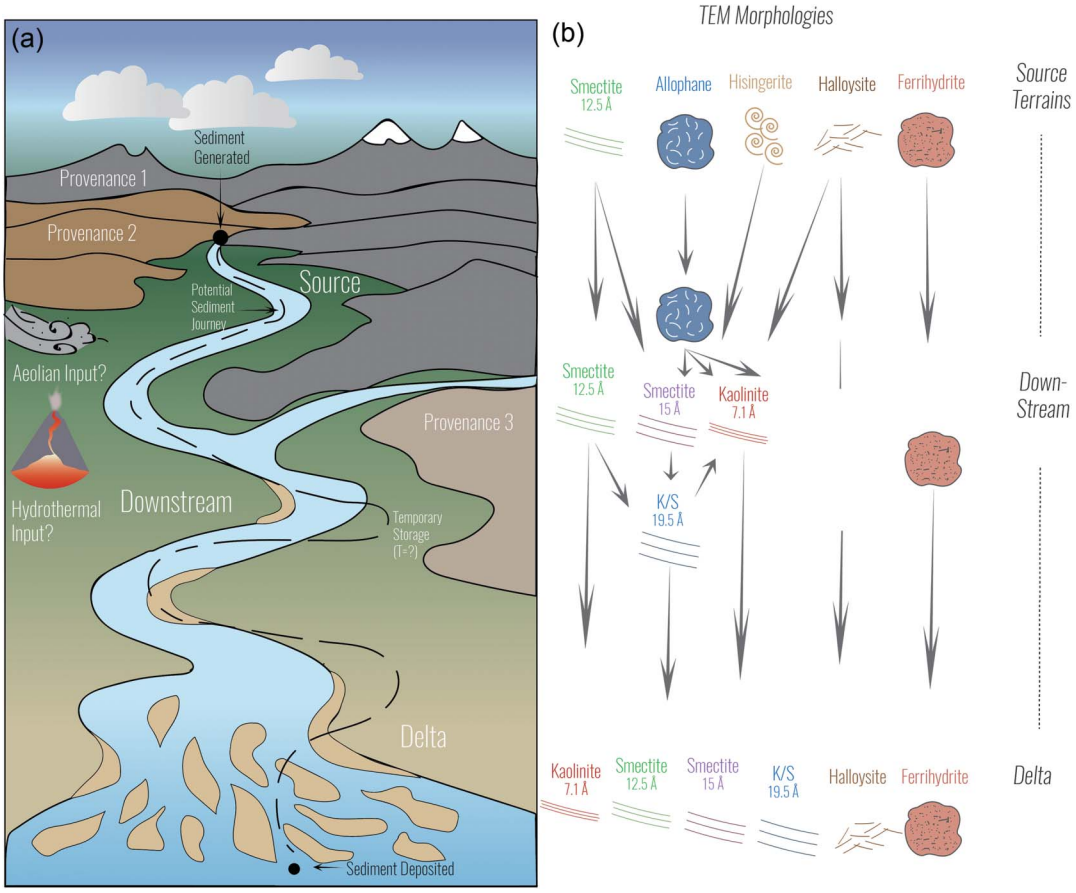

Figure 8. A sediments journey from source to sink (**a**, modified from Allen 2008) and a conceptual model (**b**) for forming amorphous materials throughout the sedimentary system. Panel (**a**) highlights the complexity of the routing system with multiple igneous provenances, variable detrital inputs (e.g., aeolian or hydrothermal), and an extended sediment pathway that includes temporary storage at sites (e.g., point bar or flood plains) along the source-to-sink system. In (**b**), gray arrows indicate a potential formational pathway for the alteration products observed in the TEM images, that are confirmed by other approaches in this study; although, there are multiple routes these phases could likely follow.

clusters, hisingerite with a curved morphology, and a halloysite-like needles. Importantly, we see that these phases vary as a function of distance from the source in the sedimentary system. In the TEM images, it appears that allophane is more abundant upstream and ferrihydrite increases downstream. This qualification is also consistent with the PDF analysis documenting the increase in ferrihydrite and amorphous materials in the downstream sediments.

The pathway for nanocrystalline and amorphous formation appears to be complex, as there may be incipient alteration products that are considered nanocrystalline or amorphous as well as later-stage phases from either continued alteration of primary phases, alteration of newly formed secondary phases, and/or the evolution of nanocrystalline or amorphous phases from one to another. Even with the high-resolution techniques employed in this study, it is difficult to rule out any of these possible scenarios, and they all likely play a role in shaping the sediment composition. However, we can conceptualize a hypothetical scenario based on our results in which all nanocrystalline and amorphous phases are initial chemical weathering products first observed in the source terrains, and some may even be precursors to the clay minerals, i.e., kaolinite and smectite, observed in the system (Fig. 8). The primary phase being altered likely controls the nanocrystalline or amorphous phase composition in this first step of the conceptual model. For example, hisingerite is more Fe-rich and is likely an incipient alteration product that formed from the weathering of olivine compared to allophane, which is more Al- and Si-rich and likely represents the initial stage of weathering a more felsic phase (e.g., plagioclase) or volcanic glass. This first step in the evolution of secondary products in the source-to-sink system is also consistent with lower smectite abundances in the source terrains compared to downstream; thus, the source terrains may only be capturing incipient alteration products. As the sediments continue downstream (Fig. 8), this chemical weathering process continues, and additional transformations occur. This secondary stage may be captured with the maturation of some nanocrystalline or amorphous products giving way to phyllosilicates. For example, halloysite has been shown to evolve to kaolinite as weathering intensity increases (Papoulis et al. 2004). Similarly, allophane has been proposed as a precursor for kaolinite during kaolinitization (e.g., Dill 2016), an intermediate weathering

product to 2:1 clay minerals, e.g., smectite (e.g., Colman 1982), and even a predecessor to halloysite through a resilication process (e.g., Koji 1989).

At this stage, alteration likely continued at temporary storage sites downstream (e.g., point bars or flood plains), during which mobile ions (e.g., Mg^{2+}) continued to be leached leaving behind immobile elements such as Fe. This elemental behavior is also consistent with the geochemistry reported by Thorpe et al. (2019), where the authors first observed an initial trend toward Al enrichment during incipient alteration and then as sediments traveled downstream, they become enriched with Fe. In the conceptual model, this elemental behavior would also favor the enrichment of ferrihydrite in the downstream sediments, as observed in the TEM and PDF patterns. During this secondary stage, we also observe the mixed-layer K/S, signifying either a hydrothermal input (either has fluvial or aeolian detritus) or our preferred interpretation of continued alteration of the secondary products along the transportation pathway. Finally, as the sediments approach the delta, the same alteration trends observed in the second stage have progressed even further, making K/S more abundant than smectite and ferrihydrite the dominant amorphous product.

Continued exploration of high-resolution techniques

SRX maps provided context to the overall elemental cycling in these Icelandic sediments. By performing coarser scans to create elemental maps, we found that Fe and Ca are widely dispersed and Co and Ni are highlighted in discrete grains in the source terrains. This elemental behavior is likely linked to the primary mineralogy, as these sediments were most enriched in mafic minerals. We suggest that Fe, Co, and Ni track individual grains of olivine and/or pyroxene while Ca is more likely associated with plagioclase. In comparison, Fe is abundant downstream but also covaries with Ca in smaller particles, a behavior we suggest signifies smectite formation based on the identification of smectite in downstream sediments via XRD, PDF, and TEM. Additionally, we observe a correlation between Mn and Fe in the downstream sediments, suggesting a redox influence as these sediments are altered downstream. Farther along in the transportation pathway, the sediments approaching the delta become more homogenous in their elemental distributions and appear to be more rounded. These observations suggest that sediments become: (1) finer grained farther downstream and (2) the downstream sediment deposits are more physically and chemically altered compared to upstream. The chemical homogenization of sediments agrees with previous work by Thorpe et al. (2019) that demonstrated the entire sediment deposits near the delta, including the coarser grained fraction (e.g., sand to pebbles), becomes more altered with less mineralogical variability among the various grain sizes. Together, this suggests that weathering and physical breakdown homogenize the sediments during transport, which increases with distance traveled in the routing system from source to sink.

In addition to elemental cycling, we also observe a unique trend in the oxidation state of Fe in both the downstream and delta sediments. During the coarse scans, we were able to identify a region that displayed a ring-like distribution of Fe. Rapid SRX XANES maps suggest a weathering front in the Icelandic sediments, with the exterior of the grains enriched in ferric iron and the cores enriched in ferrous iron. This may represent an alteration of grains within as they are transported, stored at temporary storage sites (e.g., point bar), and then re-entrained within the sediment conveyor belt. This process of continued alteration is easy to envision but is a step in the source-to-sink system that has been historically overlooked. Characterization of sediment alteration along the pathway is an ongoing area of research. Our SRX approach informs ways to advance this technique. First, we suggest using coarser scans to identify an area of interest and then focus on areas to perform more detailed scans at a higher resolution. Additionally, during the analysis, we discovered that rapid SRX XANES maps were less destructive to beam-sensitive samples than a traditional XANES scan. Finally, exploring the fate of other redox-sensitive elements in these environments will help develop a more complete sedimentary history.

Implications for Earth, current rover exploration of Mars, and the future of sample return missions

The results of this work highlight how complex the mud size fraction of sedimentary deposits can be on Earth and warrants caution in interpreting the sedimentary rock record of Mars using bulk instrument techniques. However, when rooted in a terrestrial reference framed with high-resolution approaches, we can attempt to scale these interpretations up to rover-style measurements. For example, at Gale crater, the geochemistry and mineralogy from the Curiosity rover previously suggested a modest weathering history (e.g., McLennan et al. 2014; Hurowitz et al. 2017; Rampe et al. 2017; Bristow et al. 2018; Thorpe et al. 2022). Results from this work demonstrate that in a Mars-analog cold and wet climate on Earth, the true extent of alteration may have been underestimated from coarser-resolution techniques in previous studies (e.g., Thorpe et al. 2019). If these results from Iceland are placed into a terrestrial reference frame for extending our interpretations to Mars, then this work may suggest that the elusive amorphous component of Gale crater sedimentary rocks is also composed of a natural intimate and multi-phase mixture. Moreover, if the martian X-ray amorphous component has any resemblance to the Icelandic catchment we explored, the composition of the amorphous component likely also evolves from sample to sample in the source-to-sink system and would likely be dependent on several sedimentary processes shaping the overall composition. Finally, extending the context of these results to Jezero crater, where the Perseverance rover has already discovered evidence for smectite, serpentine, and potentially vermiculite (e.g., Dehouck et al. 2023), the clay mineral story may be even more dynamic and can only be fully unraveled with these samples back on Earth and using high-resolution techniques.

The approach and techniques used in this study dealt with handling a small amount of sample mass and extracting the most geochemical and mineralogical information from it. This study emphasizes the importance of coordinated analysis using high-resolution techniques for piecing together the sedimentary history of glacio-fluvial systems in Iceland. Specifically, our results revealed that glacio-fluvial sediments from a watershed in southwest Iceland are more altered than previously reported and that the secondary nanocrystalline and amorphous assemblage is dynamic within the source-to-sink system. On Earth,

underestimating the extent of alteration in modern sediments has implications for interpreting the paleoclimate preserved in the sedimentary rock record as well as for fully understanding the geological carbon cycle, as weathering mafic sediments can be a sink for CO_2. Finally, this work not only underpins the importance of using high-resolution techniques for sample return missions but also draws a connection to current planetary missions and how we can use our high-resolution terrestrial reference frame to better interpret the sedimentary history of Mars. As we are in the golden age of sample return (e.g., asteroid samples were recently returned from Hayabusa2 and OSIRIS-REx, while Artemis III and Mars Sample Return are on the horizon), a similar methodology should be considered to characterize the composition and structure of the finest grain size fraction of future planetary materials.

Acknowledgments and Funding

The authors thank Christopher Snead for training M.T.T. to prepare microtome sections and both Cherie Achilles and Amy McAdam for many fruitful discussions on alteration products. Additionally, the authors are grateful to Milinda Abeykoon and Zak Jibrin for their help exploring the XRD data. Finally, the authors also thank associate editor, Janice Bishop, as well as Briony Horgan, F. Marc Michel, and one anonymous reviewer for greatly helping improve this manuscript with their comments and recommendations. M.T.T. acknowledges that this work was performed as part of the NASA Postdoctoral Program and was also supported by NASA under award number 80GSFC21M0002. This research used resources 28-ID-1 and 5-ID of the National Synchrotron Light Source II, a U.S. Department of Energy (DOE) Office of Science User Facility operated for the DOE Office of Science by Brookhaven National Laboratory under Contract No. DE-SC0012704.

References Cited

Achilles, C.N., Rampe, E.B., Downs, R.T., Bristow, T.F., Ming, D.W., Morris, R.V., Vaniman, D.T., Blake, D.F., Yen, A.S., McAdam, A.C., and others. (2020) Evidence for multiple diagenetic episodes in ancient fluvial-lacustrine sedimentary rocks in Gale crater, Mars. Journal of Geophysical Research: Planets, 125, e2019JE006295, https://doi.org/10.1029/2019JE006295.

Allen, P.A. (2008) From landscapes into geological history. Nature, 451, 274–276, https://doi.org/10.1038/nature06586.

Allwood, A.C., Rosing, M.T., Flannery, D.T., Hurowitz, J.A., and Heirwegh, C.M. (2018) Reassessing evidence of life in 3,700-million-year-old rocks of Greenland. Nature, 563, 241–244.

Arnalds, O. (2004) Volcanic soils of Iceland. Catena, 56, 3–20, https://doi.org/10.1016/j.catena.2003.10.002.

Ashley, H.E. (1909) The colloid matter of clay and its measurement. U.S. Geological Survey Bulletin, 388, 1–65.

Bodvarsson, G. (1961) Physical characteristics of natural heat resources in Iceland. Joekull (Reykjavik, Iceland), 11.

Bristow, T.F., Rampe, E.B., Achilles, C.N., Blake, D.F., Chipera, S.J., Craig, P., Crisp, J.A., Des Marais, D.J., Downs, R.T., Gellert, R., and others. (2018) Clay mineral diversity and abundance in sedimentary rocks of Gale crater, Mars. Science Advances, 4, eaar3330, https://doi.org/10.1126/sciadv.aar3330.

Brown, J.L. and Rich, C.I. (1968) High-resolution electron microscopy of muscovite. Science, 161, 1135–1137, https://doi.org/10.1126/science.161.3846.1135.

Bunaciu, A.A., Udriştioiu, E.G., and Aboul-Enein, H.Y. (2015) X-ray diffraction: instrumentation and applications. Critical Reviews in Analytical Chemistry, 45(4), 289–299.

Cabrol, N.A. and Grin, E.A., Eds. (2010) Searching for lakes on Mars: Four decades of exploration, p. 1–29. Lakes on Mars. Elsevier.

Caraballo, M.A., Michel, F.M., and Hochella, M.F. Jr. (2015) The rapid expansion of environmental mineralogy in unconventional ways: Beyond the accepted definition of a mineral, the latest technology, and using nature as our guide. American Mineralogist, 100, 14–25, https://doi.org/10.2138/am-2015-4749.

Chen-Wiegart, Y.C.K., Williams, G., Zhao, C., Jiang, H., Li, L., Demkowicz, M., and others. (2016) Early science commissioning results of the sub-micron resolution X-ray spectroscopy beamline (SRX) in the field of materials science and engineering. In AIP Conference Proceedings (Vol. 1764, No. 1). AIP Publishing.

Chupas, P.J., Qiu, X., Hanson, J.C., Lee, P.L., Grey, C.P., and Billinge, S.J. (2003) Rapid-acquisition pair distribution function (RA-PDF) analysis. Journal of Applied Crystallography, 36, 1342–1347, https://doi.org/10.1107/S0021889803017564).

Colman, S.M. (1982) Clay mineralogy of weathering rinds and possible implications concerning the sources of clay minerals in soils. Geology, 10, 370, https://doi.org/10.1130/0091-7613(1982)10<370:CMOWRA>2.0.CO;2.

De Andrade, V., Thieme, J., Chubar, O., and Idir, M. (2011) Simulation and optimization of the NSLS-II SRX beamline combining ray-tracing and wavefront propagation. In Advances in Computational Methods for X-ray Optics Ii (Vol. 8141, pp. 170–179). SPIE.

Dehouck, E., McLennan, S.M., Meslin, P.-Y., and Cousin, A. (2014) Constraints on abundance, composition, and nature of X-ray amorphous components of soils and rocks at Gale crater, Mars. Journal of Geophysical Research: Planets, 119, 2640–2657, https://doi.org/10.1002/2014JE004716.

Dehouck, E., Forni, O., Quantin-Nataf, C., Beck, P., Mangold, N., Royer, C., Clavé, E., Beyssac, O., Johnson, J.R., Mandon, L., and others. (2023) Overview of the Bedrock Geochemistry and Mineralogy Observed by SuperCAM during Perseverance's Delta Front Campaign, 2862 p. 54th Lunar and Planetary Science Conference, https://mars.nasa.gov/mars2020/spacecraft/instruments/supercam/for-scientists/.

Dekov, V.M., Scholten, J., Botz, R., Garbe-Schönberg, C.D., Thiry, M., Stoffers, P., and Schmidt, M. (2005) Occurrence of kaolinite and mixed-layer kaolinite/smectite in hydrothermal sediments of Grimsey Graben, Tjörnes Fracture Zone (north of Iceland). Marine Geology, 215, 159–170, https://doi.org/10.1016/j.margeo.2004.12.004.

Dill, H.G. (2016) Kaolin: Soil, rock and ore: From the mineral to the magmatic, sedimentary and metamorphic environments. Earth-Science Reviews, 161, 16–129, https://doi.org/10.1016/j.earscirev.2016.07.003.

Dixon, J.B. and McKee, T.R. (1974) Internal and external morphology of tubular and spheroidal halloysite particles. Clays and Clay Minerals, 22, 127–137, https://doi.org/10.1346/CCMN.1974.0220118.

Dixon, J.B. and Weed, S.B., Eds. (1989) Minerals in Soil Environments (SSSA Book Series), 1244 p. Soil Science Society of America.

Downs, R.T. and Hall-Wallace, M. (2003) The American Mineralogist crystal structure database. American Mineralogist, 88(1), 247–250.

Du, P., Wang, S., Yuan, P., Liu, J., Liu, D., Guo, H., Xiang, X., and Guo, X. (2022) Structure of allophanes with varied Si/Al molar ratios and implications to their differentiation on Mars. Icarus, 382, 115057, https://doi.org/10.1016/j.icarus.2022.115057.

Eggleton, R.A. and Tilley, D.B. (1998) Hisingerite: A ferric kaolin mineral with curved morphology. Clays and Clay Minerals, 46, 400–413, https://doi.org/10.1346/CCMN.1998.0460404.

Ehlmann, B.L. and Edwards, C.S. (2014) Mineralogy of the Martian surface. Annual Review of Earth and Planetary Sciences, 42(1), 291–315.

Ehlmann, B.L., Bish, D.L., Ruff, S.W., and Mustard, J.F. (2012) Mineralogy and chemistry of altered Icelandic basalts: Application to clay mineral detection and understanding aqueous environments on Mars. Journal of Geophysical Research. Planets, 117, E00J16, https://doi.org/10.1029/2012JE004156.

Filimonova, S., Kaufhold, S., Wagner, F.E., Häusler, W., and Kögel-Knabner, I. (2016) The role of allophane nano-structure and Fe oxide speciation for hosting soil organic matter in an allophanic Andosol. Geochimica et Cosmochimica Acta, 180, 284–302, https://doi.org/10.1016/j.gca.2016.02.033.

Grotzinger, J.P., Sumner, D.Y., Kah, L.C., Stack, K., Gupta, S., Edgar, L., Rubin, D., Lewis, K., Schieber, J., Mangold, N., and others. (2014) A habitable fluvio-lacustrine environment at Yellowknife Bay, Gale crater, Mars. Science, 343, 1242777, https://doi.org/10.1126/science.1242777.

Grotzinger, J.P., Gupta, S., Malin, M.C., Rubin, D.M., Schieber, J., Siebach, K., Sumner, D.Y., Stack, K.M., Vasavada, A.R., Arvidson, R.E., and others. (2015) Deposition, exhumation, and paleoclimate of an ancient lake deposit, Gale crater, Mars. Science, 350, aac7575, https://doi.org/10.1126/science.aac7575.

Hammersley, A.P., Svensson, S.O., and Thompson, A. (1994) Calibration and correction of spatial distortions in 2D detector systems. Nuclear Instruments & Methods in Physics Research Section A: Accelerators, Spectrometers, Detectors and Associated Equipment, 346, 312–321, https://doi.org/10.1016/0168-9002(94)90720-X.

Hawkins, A.B. and Pinches, G.M. (1992) Engineering description of mudrocks. Quarterly Journal of Engineering Geology, 25, 17–30, https://doi.org/10.1144/GSL.QJEG.1992.025.01.02.

Hurowitz, J.A., Grotzinger, J.P., Fischer, W.W., McLennan, S.M., Milliken, R.E., Stein, N., Vasavada, A.R., Blake, D.F., Dehouck, E., Eigenbrode, J.L., and others. (2017) Redox stratification of an ancient lake in Gale crater, Mars. Science, 356, eaah6849, https://doi.org/10.1126/science.aah6849.

Jibrin, Z.B., Achilles, C.N., Rampe, E.B., Thorpe, M.T., and McAdam, A.C. (2024) Characterization of Poorly Ordered Materials in Mars Analog Mixtures: Implications for Mars Sample Return. 55th Lunar and Planetary Science Conference, Abstract 2111.

Klug, H.P. and Alexander, L.E. (1974) X-ray Diffraction Procedures: For Polycrystalline and Amorphous Materials, 2nd edition, 992 p. Wiley.

Kogure, T. (2016) Characterisation of halloysite by electron microscopy. Developments in Clay Science, 7, 92–114. Elsevier.

Koji, W. (1989) Allophane and imogolite. In B. Dixon and S.B. Weed, Eds., Minerals in Soil Environments, Vol. 1, p. 1051–1087.

Lee, S. and Xu, H. (2020) Using complementary methods of synchrotron radiation powder diffraction and pair distribution function to refine crystal structures with high quality parameters—A review. Minerals, 10, 124, https://doi.org/10.3390/min10020124.

Lee, S., Xu, H., and Xu, H. (2022) Reexamination of the structure of opal-A: A combined study of synchrotron X-ray diffraction and pair distribution function analysis. American Mineralogist, 107, 1353–1360, https://doi.org/10.2138/am-2022-8017.

Lemmon, M.T., Guzewich, S.D., McConnochie, T., de Vicente-Retortillo, A., Martínez, G., Smith, M.D., Bell, J.F. III, Wellington, D., and Jacob, S. (2019) Large dust aerosol sizes seen during the 2018 martian global dust event by the Curiosity rover. Geophysical Research Letters, 46, 9448–9456, https://doi.org/10.1029/2019GL084407.

Liu, D., Tian, Q., Yuan, P., Du, P., Zhou, J., Li, Y., Bu, H., and Zhou, J. (2019) Facile sample preparation method allowing TEM characterization of the stacking structures and interlayer spaces of clay minerals. Applied Clay Science, 171, 1–5, https://doi.org/10.1016/j.clay.2019.01.019.

Malla, P.B. and Komameni, S. (1990) High-resolution transmission electron microscopy (HRTEM) in the study of clays and soils. In B.A. Stewart, Eds., Advances in Soil Science, Vol. 12, 159–186. Springer.

Mangold, N., Baratoux, D., Arnalds, O., Bardintzeff, J.M., Platevoet, B., Grégoire, M., and Pinet, P. (2011) Segregation of olivine grains in volcanic sands in Iceland and implications for Mars. Earth and Planetary Science Letters, 310, 233–243, https://doi.org/10.1016/j.epsl.2011.07.025.

Markússon, S.H. and Stefánsson, A. (2011) Geothermal surface alteration of basalts, Krýsuvík Iceland—Alteration mineralogy, water chemistry and the effects of acid supply on the alteration process. Journal of Volcanology and Geothermal Research, 206, 46–59, https://doi.org/10.1016/j.jvolgeores.2011.05.007.

McLennan, S.M., Anderson, R.B., Bell, J.F. III, Bridges, J.C., Calef, F. III, Campbell, J.L., Clark, B.C., Clegg, S., Conrad, P., Cousin, A., and others. (2014) Elemental geochemistry of sedimentary rocks at Yellowknife Bay, Gale crater, Mars. Science, 343, 1244734, https://doi.org/10.1126/science.1244734.

McLennan, S.M., Grotzinger, J.P., Hurowitz, J.A., and Tosca, N.J. (2019) The sedimentary cycle on early Mars. Annual Review of Earth and Planetary Sciences, 47, 91–118, https://doi.org/10.1146/annurev-earth-053018-060332.

Meunier, A. (2005) Clays, 279 p. Springer.

Modena, M.M., Rühle, B., Burg, T.P., and Wuttke, S. (2019) Nanoparticle characterization: What to measure? Advanced Materials, 31, 1901556, https://doi.org/10.1002/adma.201901556.

Moore, D.M. and Reynolds, R.J. Jr. (1989) X-ray Diffraction and the Identification and Analysis of Clay Minerals, 352 p. Oxford University Press.

Nesbitt, H.W., Young, G.M., McLennan, S.M., and Keays, R.R. (1996) Effects of chemical weathering and sorting on the petrogenesis of siliciclastic sediments, with implications for provenance studies. The Journal of Geology, 104, 525–542, https://doi.org/10.1086/629850.

Papoulis, D., Tsolis-Katagas, P., and Katagas, C. (2004) Progressive stages in the formation of kaolin minerals of different morphologies in the weathering of plagioclase. Clays and Clay Minerals, 52, 275–286, https://doi.org/10.1346/CCMN.2004.0520303.

Petkov, V. (2008) Nanostructure by high-energy X-ray diffraction. Materials Today, 11, 28–38, https://doi.org/10.1016/S1369-7021(08)70236-0.

——— (2012) Pair distribution functions analysis. In E.N. Kaufmann, Ed., Characterization of Materials, 1361 p. Wiley.

Pettijohn, F.J. (1975) Sedimentary Rocks, Volume 3, 628 p. Harper & Row.

Prothero, D.R. and Schwab, F. (2004) Sedimentary Geology. W.H. Freeman and Company.

Putnam, A.R., Siebach, K.L., Bedford, C.C., Simpson, S.L., Thorpe, M.T., Tamborski, J.J., and Rampe, E.B. (2024) Ice-marginal volcanic sequence in Iceland found on a nondescript gradual hillslope: An unexpected record of ice thickness late in deglaciation. Journal of Volcanology and Geothermal Research, 455, 108195.

Qiu, X., Thompson, J.W., and Billinge, S.J. (2004) PDFgetX2: A GUI-driven program to obtain the pair distribution function from X-ray powder diffraction data. Journal of Applied Crystallography, 37, 678, https://doi.org/10.1107/S0021889804011744.

Rampe, E.B., Ming, D.W., Blake, D.F., Bristow, T.F., Chipera, S.J., Grotzinger, J.P., Morris, R.V., Morrison, S.M., Vaniman, D.T., Yen, A.S., and others. (2017) Mineralogy of an ancient lacustrine mudstone succession from the Murray formation, Gale crater, Mars. Earth and Planetary Science Letters, 471, 172–185, https://doi.org/10.1016/j.epsl.2017.04.021.

Rampe, E.B., Horgan, B.H.N., Smith, R.J., Scudder, N.A., Bamber, E.R., Rutledge, A.M., and Christoffersen, R. (2022) A mineralogical study of glacial flour from Three Sisters, Oregon: An analog for a cold and icy early Mars. Earth and Planetary Science Letters, 584, 117471, https://doi.org/10.1016/j.epsl.2022.117471.

Sánchez-García, L., Carrizo, D., Molina, A., Muñoz-Iglesias, V., Lezcano, M.Á., Fernández-Sampedro, M., Parro, V., and Prieto-Ballesteros, O. (2020) Fingerprinting molecular and isotopic biosignatures on different hydrothermal scenarios of Iceland, an acidic and sulfur-rich Mars analog. Scientific Reports, 10, 21196, https://doi.org/10.1038/s41598-020-78240-2.

Schindler, M., Michel, S., Batcheldor, D., and Hochella, M.F. Jr. (2019) A nanoscale study of the formation of Fe-(hydr) oxides in a volcanic regolith: Implications for the understanding of soil forming processes on Earth and Mars. Geochimica et Cosmochimica Acta, 264, 43–66, https://doi.org/10.1016/j.gca.2019.08.008.

Smith, R.J. and Horgan, B.H.N. (2021) Nanoscale variations in natural amorphous and nanocrystalline weathering products in mafic to intermediate volcanic terrains on Earth: Implications for amorphous detections on Mars. Journal of Geophysical Research: Planets, 126, e2020JE006769, https://doi.org/10.1029/2020JE006769.

Smith, R.J., McLennan, S.M., Achilles, C.N., Dehouck, E., Horgan, B.H.N., Mangold, N., Rampe, E.B., Salvatore, M., Siebach, K.L., and Sun, V. (2021) X-ray amorphous components in sedimentary rocks of Gale crater, Mars: Evidence for ancient formation and long-lived aqueous activity. Journal of Geophysical Research: Planets, 126, e2020JE006782. https://doi.org/10.1029/2020JE006782.

Smith, R.J., McLennan, S.M., Sutter, B., Rampe, E.B., Dehouck, E., Siebach, K.L., Horgan, B.H.N., Sun, V., McAdam, A., Mangold, N., and others. (2022) X-ray amorphous sulfur-bearing phases in sedimentary rocks of Gale crater, Mars. Journal of Geophysical Research: Planets, 127, e2021JE007128. https://doi.org/10.1029/2021JE007128.

Środoń, J. (1999) Nature of mixed-layer clays and mechanisms of their formation and alteration. Annual Review of Earth and Planetary Sciences, 27, 19–53, https://doi.org/10.1146/annurev.earth.27.1.19.

Suquet, H., De La Calle, C., and Pezerat, H. (1975) Swelling and structural organization of saponite. Clays and Clay Minerals, 23, 1–9, https://doi.org/10.1346/CCMN.1975.0230101.

Terban, M.W. and Billinge, S.J.L. (2021) Structural analysis of molecular materials using the pair distribution function. Chemical Reviews, 122, 1208–1272, https://doi.org/10.1021/acs.chemrev.1c00237.

Thorpe, M.T., Hurowitz, J.A., and Dehouck, E. (2019) Sediment geochemistry and mineralogy from a glacial terrain river system in southwest Iceland. Geochimica et Cosmochimica Acta, 263, 140–166, https://doi.org/10.1016/j.gca.2019.08.003.

Thorpe, M.T., Hurowitz, J.A., and Siebach, K.L. (2021) Source-to-sink terrestrial analogs for the paleoenvironment of Gale crater, Mars. Journal of Geophysical Research: Planets, 126, e2020JE006530, https://doi.org/10.1029/2020JE006530.

Thorpe, M.T., Bristow, T.F., Rampe, E.B., Tosca, N.J., Grotzinger, J.P., Bennett, K.W., Achilles, C.N., Blake, D.F., Chipera, S.J., Downs, G., and others. (2022) Mars Science Laboratory CheMin data from the Glen Torridon region and the significance of lake-groundwater interactions in interpreting mineralogy and sedimentary history. Journal of Geophysical Research: Planets, 127, e2021JE007099, https://doi.org/10.1029/2021JE007099.

Tosca, N.J., Agee, C.B., Cockell, C.S., Glavin, D.P., Hutzler, A., Marty, B., McCubbin, F.M., Regberg, A.B., Velbel, M.A., Kminek, G., and others. (2022) Time-sensitive aspects of Mars Sample Return (MSR) science. Astrobiology, 22, iv-S-241, https://doi.org/10.1089/ast.2021.0115.

Wada, K. (1987) Minerals formed and mineral formation from volcanic ash by weathering. Chemical Geology, 60, 17–28, https://doi.org/10.1016/0009-2541(87)90106-9.

Wada, K., Arnalds, O., Kakuto, Y., Wilding, L.P., and Hallmark, C.T. (1992) Clay minerals of four soils formed in eolian and tephra materials in Iceland. Geoderma, 52, 351–365, https://doi.org/10.1016/0016-7061(92)90046-A.

Warner, N.H. and Farmer, J.D. (2010) Subglacial hydrothermal alteration minerals in Jökulhlaup deposits of Southern Iceland, with implications for detecting past or present habitable environments on Mars. Astrobiology, 10, 523–547, https://doi.org/10.1089/ast.2009.0425.

Manuscript received December 20, 2023
Manuscript accepted February 19, 2025
Accepted manuscript online March 6, 2025
Manuscript Handled by Janice Bishop

Endnotes:

[1]Deposit item AM-25-119290. Online Materials are free to all readers. Go online, via the table of contents or article view, and find the tab or link for supplemental materials.